JOURNAL OF MATERIALS SCIENCE 21 (1986) 1258–1268

Superconducting and electrical properties of amorphous zirconium–transition metal binary alloys

A. INOUE, K. MATSUZAKI, T. MASUMOTO
The Research Institute for Iron, Steel and Other Metals, Tohoku University, Sendai 980, Japan
H. S. CHEN
ATT Bell Laboratories, 600 Mountain Avenue, Murray Hill, New Jersey 07974, USA

In order to clarify the compositional effect on the superconductivity of zirconium–transition metal (M) binary amorphous alloys, the superconducting properties and electrical resistance of the alloys were examined as functions of the concentration, group number and periodicity of the M elements. T_c for $Zr_{75}M_{25}$ alloys rises in the order Ru > Rh > Ir > Co > Os > Ni > Pt > Cu > Pd > Fe > Au, i.e. as the group number decreases when the periodicity belongs to the 5th period, and with decreasing M content for $Zr_{100-x}M_x$ alloys. The high T_c attained in the present work is 4.55 K for $Zr_{80}Rh_{20}$, 4.38 K for $Zr_{75}Rh_{25}$ and 4.47 K for $Zr_{75}Ru_{25}$. The temperature gradient of the upper critical magnetic field (H_{c2}) near the transition temperature (T_c) tends to increase with increasing zirconium content, and the resistive state due to the flux flow phenomena appears in a wide sweeping field. Following the sharp and large decrease of the flux flow resistance due to a peak effect, the resistance recovers sharply near H_{c2}. The peak effect was found to occur more distinctly for the alloys containing a magnetic element of iron or cobalt, probably because of the suppression of the pair-breaking effect due to magnetic scattering by the application of the high field near H_{c2}. The dominating factor for the compositional effect on T_c is inferred to originate from the variation of λ through ω for $Zr_{100-x}M_x$ alloys and from that of λ through $N(E_f)$ for $Zr_{75}M_{25}$ alloys. Additionally, it has been found for the Zr–M amorphous alloys that the electrical resistivity $\varrho(T)$ exhibits a maximum value at temperature ranging from $2T_c$ to $3T_c$, suggesting that the hump phenomenon in $\varrho(T)$ appeared through the generation of the superconducting fluctuations. The temperature coefficient of resistivity (tcr) defined by $1/R_{250}(dR/dT)$ shows negative values ranging from 1.05×10^{-4} to $1.75 \times 10^{-4}\,K^{-1}$ and T_c was found to rise through the increase in λ with the increase in the negative value of the tcr.

1. Introduction

A large part of the investigations on the superconducting properties of amorphous alloys have been focused on the metal–metal type alloys of Zr–M (M = cobalt [1–6], nickel [2, 3, 5, 7, 8–10], copper [1, 2, 5, 7, 11] or rhodium [12, 13] etc.) systems despite low values of the superconducting transition temperature (T_c), because the amorphization of the Zr–M alloys by a conventional melt-spinning technique is relatively easy and the simple alloy component provides a unique opportunity to study the superconducting mechanism of an amorphous alloy. Previous results [1–13] have indicated that the T_c value rises with increasing zirconium content, in the ranges below about 3.2 K for $Zr_{100-x}Cu_x$ alloys and 3.9 K for $Zr_{100-x}Ni_x$ alloys, reflecting the variation of the electronic density of states at the Fermi level with alloy composition. However, almost all the previous investigations on the superconducting properties of zirconium–transition metal (M) amorphous alloys have been performed for individual alloy systems by different researchers. There is little systematic information on the effects of the group number and periodicity in the Periodic Table of solute M elements on the superconducting and electrical properties such as T_c, $J_c(H)$, $H_{c2}(T)$, $\varrho_f(H)$ and $\varrho(T)$ of the Zr–M amorphous alloys, as well as their formation ranges. Most recently, the Zr–Rh and Zr–Ru amorphous alloys have been found [14] to exhibit many excellent characteristics, which are not expected for conventional crystalline superconductors, as sensing elements in a liquid-helium level indicator. A level indicator with sensing element made of amorphous Zr–Rh or Zr–Ru ribbon has been practically used in various kinds of commercial cryogenic vessels [15]. Accordingly, from scientific and engineering points of view it is desirable to obtain systematic information on the superconducting and electrical properties of Zr–M amorphous alloys. This paper intends (1) to clarify the composition range in which the amorphous phase is formed in Zr–M binary alloys containing various transition M metals, (2) to examine the change in the superconducting properties

0022–2461/86 $03.00 + .12

with M content for $Zr_{100-x}M_x$ amorphous alloys and with the group number and periodicity of M elements for $Zr_{75}M_{25}$ amorphous alloys, (3) to decide a dominant factor for such changes in the superconducting properties, and (4) to investigate the correlation between the superconducting characteristics and the temperature dependence of normal electrical resistance.

2. Experimental procedure

Mixtures of 99.6 wt % pure zirconium and pure M (M = iron, cobalt, nickel, copper, ruthenium, rhodium, palladium, osmium, iridium, platinum or gold) metal were melted under a purified and gettered argon atmosphere on a water-cooled copper mould in an arc furnace. The weight of the mixture melted in one run was about 30 g. The ingots were repeatedly turned over and remelted to ensure homogeneity. The compositions of alloys reported are the nominal ones since the losses during melting were negligible.

Continuous ribbon specimens of about 1 to 2 mm width and 0.02 to 0.03 mm thickness were prepared from these mixed alloys under a purified argon atmosphere using a single-roller melt-spinning apparatus. The amorphous nature of the as-quenched ribbon was confirmed by X-ray diffractometer using Cu$K\alpha$ radiation and with a transmission electron microscopy.

All measurements of superconducting and electrical properties, transition temperature T_c, critical current density $J_c(H)$, upper critical magnetic field $H_{c2}(T)$, flux flow resistivity $\varrho_f(H)$ and electrical resistivity $\varrho(T)$ were done resistively using a conventional four-probe technique. The critical current was defined as the threshold current at which no zero voltage ($> 1\ \mu V$) was first detected. The magnetic field up to 9 T was applied transversely to the specimen surface and excited current. The temperature was measured using a calibrated germanium thermometer at temperatures below about 90 K and a calibrated diode thermometer in the higher temperature range with accuracy better than ± 0.01 K at temperatures below 90 K and ± 0.1 K at the higher temperatures. The Young's modulus sound velocity (V_E) was measured at 100 kHz using a pulse-echo technique [16] on amorphous ribbons about 50 to 100 cm long and the Young's modulus (E) is given by $E = \varrho V_E^2$, where ϱ is the density of the amorphous ribbons. The measurement was conducted at ambient temperatures. The maximum scatter of the velocity measurement was $\pm 0.5\%$ due to the uncertainties in the length measurements. The density of the amorphous ribbons was measured for some of the alloy compositions by the Archimedean method.

3. Results

3.1. Formation range of amorphous phase

Fig. 1 shows the composition ranges in which the amorphous phase was found to form without any trace of crystallinity in the Zr–M (M = iron, cobalt, nickel, copper, ruthenium, rhodium, palladium, osmium, iridium, platinum or gold) binary systems containing M elements less than 40 at %. The amorphous phase is formed in each range centred around 25 at % M, e.g. 20 to 40% Fe, 20 to 40% Co, 15 to 40% Ni, 25 to 40% Cu, 25% Ru, 20 to 35% Rh, 25 to 35% Pd, 20 to 30% Os, 20 to 30% Ir, 20 to 25% Pt and 25 to 35% Au. Judging from the fact [17] that the equilibrium phase diagrams of these alloys have a eutectic point in the vicinity of 25 at % M, the amorphous phase formation appears to be easier in the composition range near a eutectic point where the melting temperature of the alloys is lower. This tendency is consistent with the previous empirical rule (e.g. [18]) on the amorphous phase-forming tendency. The amorphous phase with the highest zirconium contentration is obtained for Zr–Ni alloys, e.g. $Zr_{85}Ni_{15}$. The formation range of the amorphous phase becomes narrower in the order of Ni > Fe ≃ Co > Cu > Rh > Pd ≃ Os ≃ Ir ≃ Au > Pt > Ru and Zr–Ru alloys become amorphous only in the vicinity of 25 at % Ru. The broken lines for Zr–Rh, Zr–Os and Zr–Ir alloys in Fig. 1 indicate that the melting temperature of the alloys is too high to obtain amorphous ribbon samples by the present melt-spinning apparatus with conventional high-frequency coil. All the amorphous ribbons produced by melt-quenching possess a good ductility which is tested by a 180° bending and remain ductile upon ageing at room temperature for all the alloys except Zr–Au.

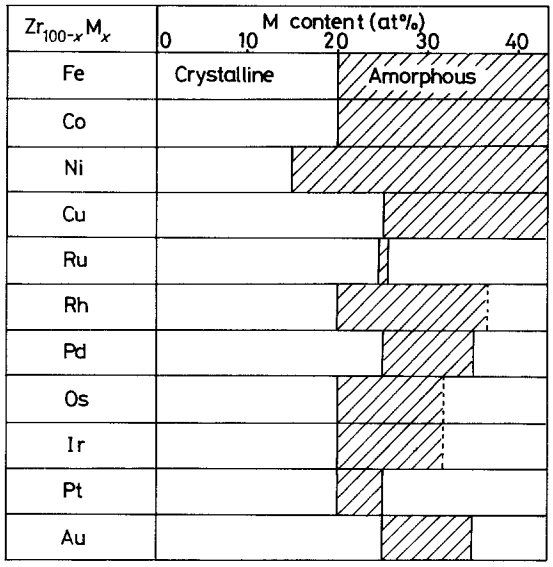

Figure 1 Composition range for the formation of an amorphous phase in the Zr–M (M = Fe, Co, Ni, Cu, Ru, Rh, Pd, Os, Ir, Pt or Au) system.

3.2. Superconducting transition temperature (T_c)

As typical examples of the transition behaviour from superconducting to normal state for Zr–M amorphous alloys, the normalized electrical resistance near T_c for Zr–Co and Zr–Ir alloys is shown in Fig. 2. The transition occurs very sharply with a temperature width of less than 0.1 K. The transition temperature (T_c) rises monotonically with decreasing cobalt or iridium content. Fig. 3 shows T_c and transition width (ΔT_c) as a function of M content of all the Zr–M (M = Fe, Co, Ni, Cu, Ru, Rh, Pd, Os, Ir, Pt or Au) amorphous alloys examined. T_c is the temperature corresponding to $R/R_n = 0.5$, where R_n is the

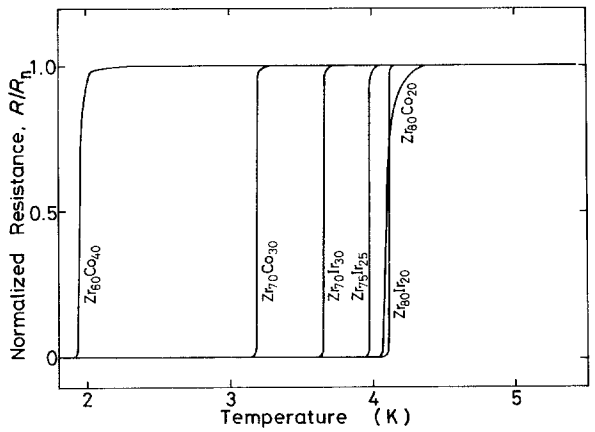

Figure 2 Normalized electrical resistance, R/R_n, as a function of temperature for $Zr_{100-x}Co_x$ and $Zr_{100-x}Ir_x$ amorphous alloys.

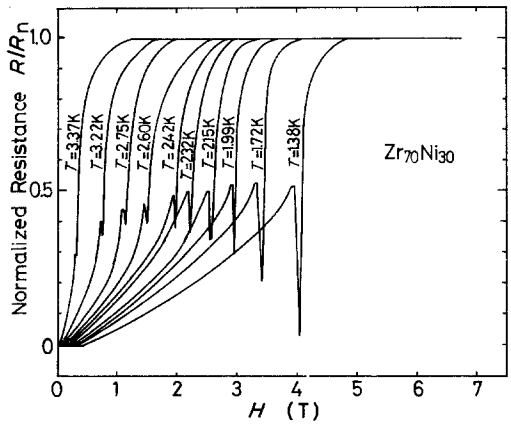

Figure 4 Electrical resistance as a function of magnetic field at various temperatures for a $Zr_{70}Ni_{30}$ amorphous alloy.

resistance in the normal state. The ΔT_c represented by a vertical bar in the figure shows the temperature interval between 0.1 and 0.9 R/R_n. As shown in Fig. 3, T_c rises with decreasing M content from 2.17 K at 25% Fe to 2.93 K at 20% Fe, 1.95 K at 40% Co to 4.11 K at 20% Co, 2.39 K at 40% Ni to 4.15 K at 15% Ni, 1.90 K at 40% Cu to 3.20 K at 25% Cu, 4.47 K at 25% Ru, 3.98 K at 35% Rh to 4.55 K at 20% Rh, 2.27 K at 35% Pd to 3.31 K at 25% Pd, 3.50 K at 30% Os to 3.97 K at 20% Os, 3.67 K at 30% Ir to 4.13 K at 20% Ir, 3.31 K at 25% Pt to 3.64 K at 20% Pt and 1.68 K at 30% Au to 1.99 K at 25% Au. It is noted that only the alloys, $Zr_{80}Rh_{20}$ (T_c = 4.55 K), $Zr_{75}Rh_{25}$ (T_c = 4.38 K) and $Zr_{75}Ru_{25}$ (T_c = 4.47 K), exhibit T_c higher than the boiling temperature of liquid helium ($\simeq$ 4.2 K).

For the series of $Zr_{75}M_{25}$ amorphous alloys (see Fig. 3), T_c is lower in the order Ru > Rh > Ir > Co > Os > Ni > Pt > Cu > Pd > Fe > Au. When such a change in T_c with M elements is compared in the same period, T_c is lowered in the order Co > Ni > Cu > Fe in the fourth period, Ru > Rh > Pd in the fifth period and Ir > Os > Pt > Au in the sixth period. The results described above indicate that the Zr–M amorphous alloys tend to exhibit a higher T_c value, when the M elements belong to a smaller group number and to the same period as that of zirconium. Only Zr–Fe and Zr–Os alloys exhibit an exceptional tendency.

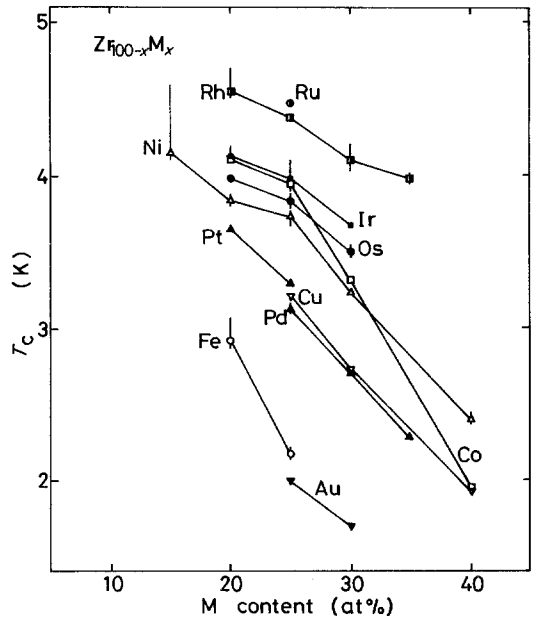

Figure 3 M concentration dependences of the superconducting transition temperature, T_c, and the transition width, ΔT_c, for $Zr_{100-x}M_x$ (M = Fe, Co, Ni, Cu, Ru, Rh, Pd, Os, Ir, Pt or Au) amorphous alloys.

3.3. Upper critical magnetic field, H_{c2}

As an example, Fig. 4 shows, for $Zr_{70}Ni_{30}$ amorphous alloy, the transition curves from superconducting to normal state through superconducting mixed state under a current density of 2.1 $\times$ 10^4 A m^{-2}. Resistive states are seen in a wide range of fields, following the sharp decrease of the resistance due to a peak effect as the field approaches H_{c2}. The occurrence of the resistive states has been interpreted as due to the flux flow phenomenon [19–21]. A similar flux flow phenomenon in the ϱ–H relation was found to occur for all the Zr–M amorphous alloys. However, the peak effect is more pronounced for the Zr–Fe and Zr–Co amorphous alloys containing magnetic elements as exemplified for $Zr_{75}Fe_{25}$ in Fig. 5. The complete disappearance of the resistivity of $Zr_{75}Fe_{25}$ alloy in the high field near H_{c2} is noted particularly. The reason for the recovery is inferred to be due to the suppression of a pair-breaking effect in superconducting nature due to magnetic scattering by the application of the high fields near H_{c2}. The temperature dependence of H_{c2} for $Zr_{75}M_{25}$ amorphous alloys is shown in Fig. 6 based on

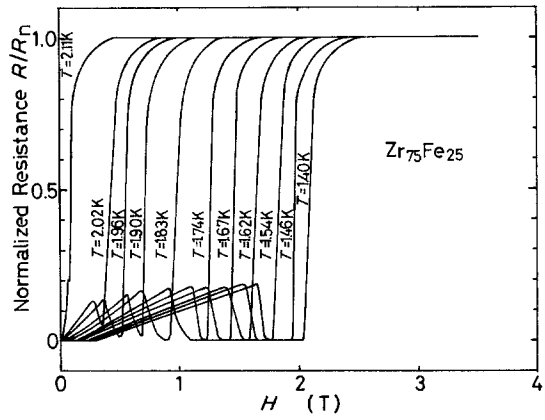

Figure 5 Electrical resistance as a function of magnetic field at various temperatures for a $Zr_{75}Fe_{25}$ amorphous alloy.

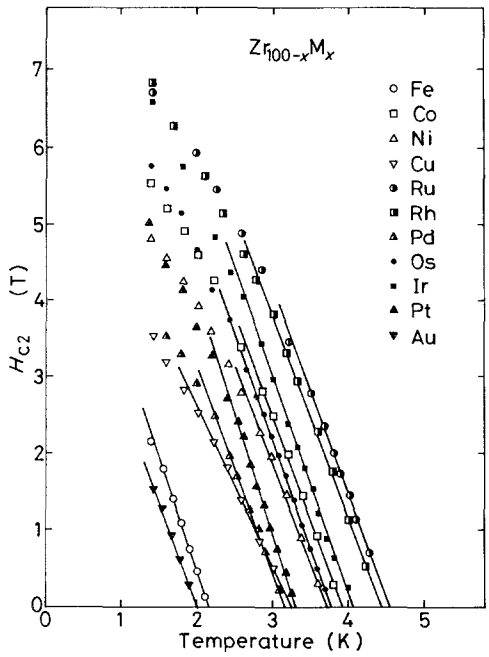

Figure 6 The upper critical magnetic field H_{c2} at various temperatures for $Zr_{75}M_{25}$ (M = Fe, Co, Ni, Cu, Ru, Rh, Pd, Os, Ir, Pt or Au) amorphous alloys. The solid lines represent a linear extrapolation at T_c.

the data exemplified in Figs. 5 and 6. Here H_{c2} is defined to be the applied magnetic field at which the resistance of the samples begins to deviate from its normal value. The solid lines of Fig. 6 represent a linear extrapolation near T_c. H_{c2} increases linearly with lowering temperature in the range above $t = T/T_c = 0.6$–0.7, but it shows negative deviation from the linear relation at low temperatures. Fig. 7 shows the temperature gradient of H_{c2} near T_c, $(dH_{c2}/dT)_{T_c}$, for $Zr_{100-x}M_x$ amorphous alloys as a function of M content. The gradient is higher than $2.5\,T\,K^{-1}$ for almost all the alloys and tends to increase with decreasing M content for all the alloys except Zr–Fe alloys. The gradients of $Zr_{80}Pt_{20}$ and $Zr_{75}Fe_{25}$ alloys are as high as 3.10 to $3.15\,T\,K^{-1}$.

3.4. Critical current density, J_c

As typical examples, the critical current density,

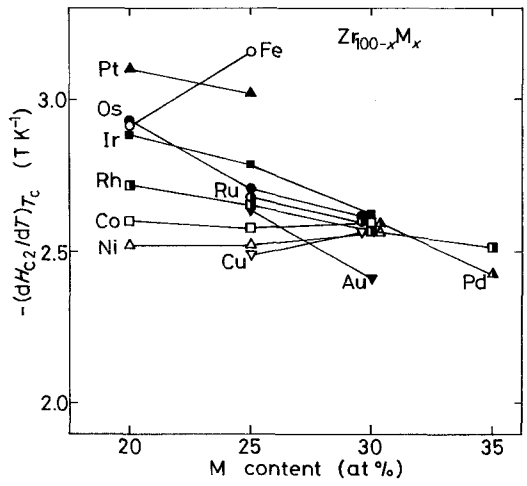

Figure 7 M concentration dependence of the upper critical field gradient at T_c, $(dH_{c2}/dT)_{T_c}$, for $Zr_{100-x}M_x$ (M = Fe, Co, Ni, Cu, Ru, Rh, Pd, Os, Ir, Pt or Au) amorphous alloys.

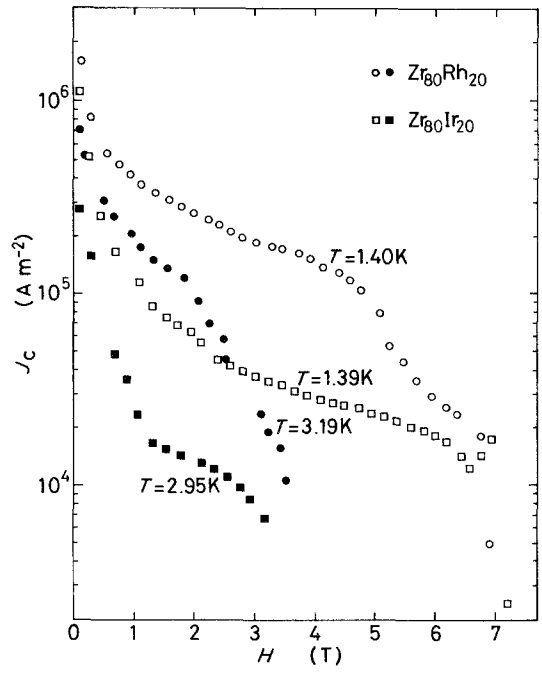

Figure 8 Critical current density, J_c, for $Zr_{80}Rh_{20}$ and $Zr_{80}Ir_{20}$ amorphous alloys as a function of magnetic field.

$J_c(H)$, as a function of external applied magnetic field is shown in Fig. 8 for $Zr_{80}Rh_{20}$ and $Zr_{80}Ir_{20}$. The value of J_c is as low as about $10^6\,A\,m^{-2}$ even at a low temperature of $\simeq 1.4$ K in the absence of applied field, and decreases rapidly with increasing applied field. For example, at $H = 5$ T at $\simeq 1.4$ K, J_c is of the order of $9 \times 10^4\,A\,m^{-2}$ for the Zr–Rh and $2 \times 10^4\,A\,m^{-2}$ for the Zr–Ir. Such small values of $J_c(H)$ indicate that the flux pinning force in the Zr–M amorphous alloys is rather weak, because atomic configurations in the amorphous phase are distorted on a scale equal to an interatomic distance (0.2 to 0.5 nm) being much smaller than the coherence length ($\simeq 7$ to 8 nm).

In order to investigate the effect of M content on $J_c(H)$, the $J_c(H)$ values of $Zr_{80}Rh_{20}$ and $Zr_{75}Rh_{25}$ amorphous alloys measured at a same reduced

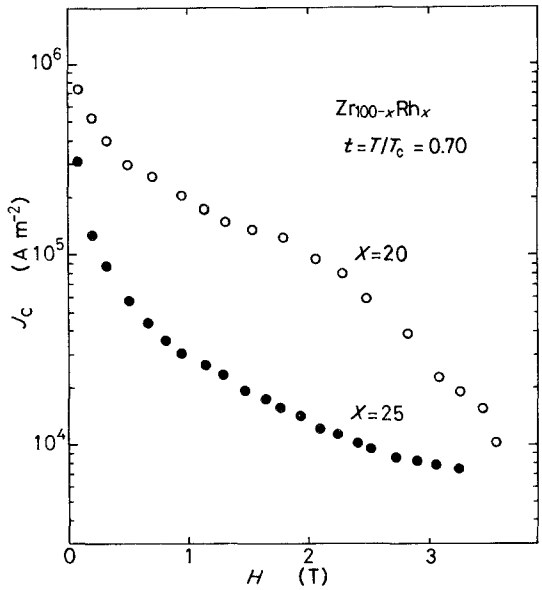

Figure 9 Critical current density, J_c, at the same reduced temperature $t = T/T_c = 0.70$ as a function of magnetic field for $Zr_{80}Rh_{20}$ and $Zr_{75}Rh_{25}$ amorphous alloys.

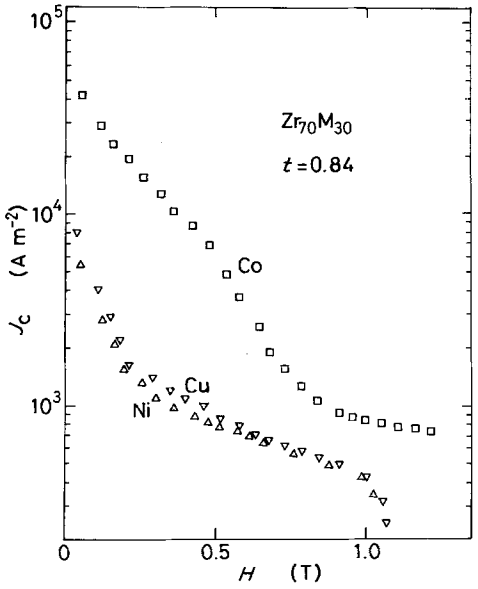

Figure 10 Critical current density, J_c, at the same reduced temperature $t = T/T_c = 0.84$ as a function of magnetic field for $Zr_{70}M_{30}$ (M = Co, Ni or Cu) amorphous alloys.

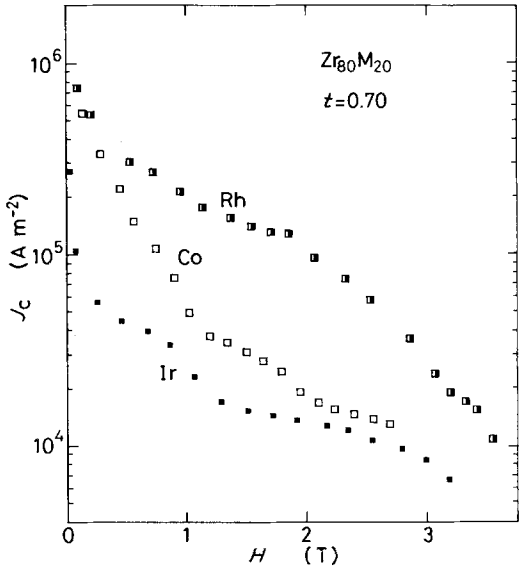

Figure 12 Critical current density, J_c, at the same reduced temperature $t = T/T_c = 0.70$ as a function of magnetic field for $Zr_{80}M_{20}$ (M = cobalt, rodium or iridium) amorphous alloys.

temperature ($t = T/T_c = 0.7$) are plotted in Fig. 9. The $J_c(H)$ is higher for $Zr_{80}Rh_{20}$ than for $Zr_{75}Rh_{25}$ in the whole magnetic field, indicating that the fluxoid pinning force is larger for the zirconium-rich alloy. The effect of the group number on $J_c(H)$ is shown in Fig. 10 for $Zr_{70}M_{30}$ alloys containing M = cobalt, nickel or copper in the fourth period and in Fig. 11 for $Zr_{75}M_{25}$ alloys containing M = ruthenium, rhodium or palladium in the fifth period. As seen in these figures, the $J_c(H)$ decreases in the order Co > Ni $\simeq$ Cu in the former period and Ru > Rh > Pd in the latter period. In the sixth period, the $J_c(H)$ at $t = 0.7$ for $Zr_{80}M_{20}$ amorphous alloys decreases in the order Os > Ir > Pt (not shown). In summary, the decrease in the group number of M elements causes an increase in fluxoid pinning force of the Zr–M amorphous alloys. The variation in $J_c(H)$ of $Zr_{80}M_{20}$ (M = Co, Rh or Ir) amorphous alloys with the periodicity is shown in Fig. 12. $J_c(H)$ decreases in the order Rh > Co > Ir, i.e. fifth > fourth > sixth, in accordance with the order of T_c. As shown in Figs. 9 to 12, the change in $J_c(H)$ of amorphous Zr–M alloys with the group number and periodicity of M elements even at the same reduced temperature agrees well with that of T_c.

3.5. Electrical resistivity

As an example, Fig. 13 shows the electrical resistance $R(T)$ of an amorphous $Zr_{75}Ir_{25}$ alloy in the range from 4.2 to 250 K. As the temperature rises, the electrical resistance increases rapidly just above T_c, exhibits a maximum value at about 12 K and then decreases. The $R(T)$ of the Zr–Ir alloy shows a large negative

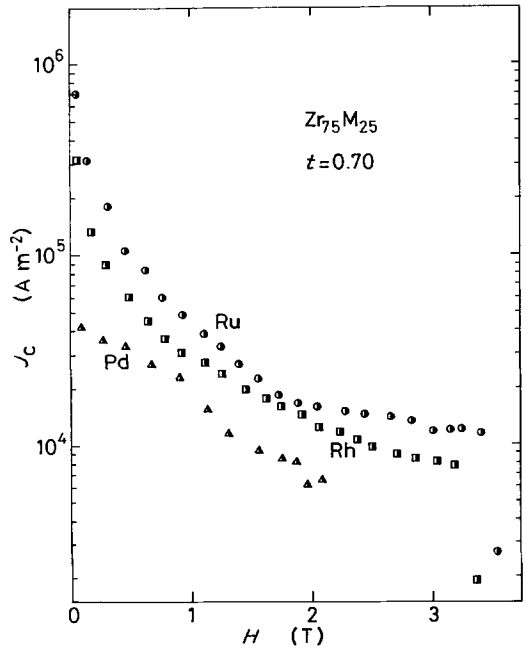

Figure 11 Critical current density, J_c, at the same reduced temperature $t = T/T_c = 0.70$ as a function of magnetic field for $Zr_{75}M_{25}$ (M = ruthenium, rhodium or palladium) amorphous alloys.

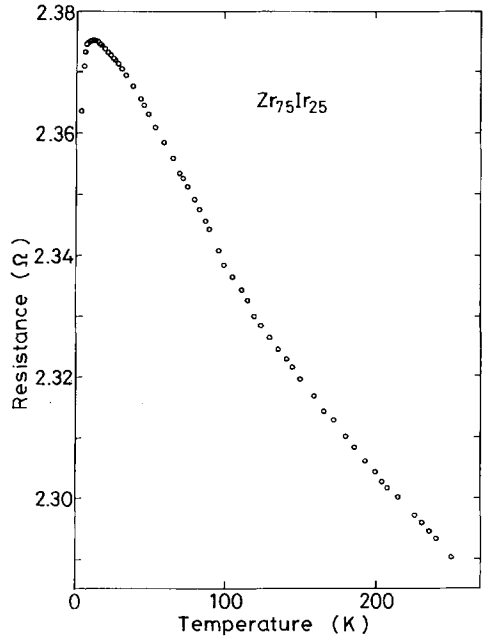

Figure 13 Normalized electrical resistance R/R_n of a $Zr_{75}Ir_{25}$ amorphous alloy as a function of temperature.

TABLE I The temperature at which the electrical resistance exhibits a maximum value, T_{max}, and the temperature coefficient of resistivity (tcr) at 250 K, $1/R_{250}(dR/dT)$, for $Zr_{100-x}M_x$ (M = Co, Ni, Ru, Rh, Pd, Ir or Pt) amorphous alloys

Alloy	T_{max} (K)	tcr (10^{-4} K^{-1})
$Zr_{80}Co_{20}$	–	−1.75
$Zr_{75}Co_{25}$	–	−1.55
$Zr_{70}Co_{30}$	–	−1.05
$Zr_{80}Ni_{20}$	9.81	−1.68
$Zr_{75}Ni_{25}$	8.69	−1.60
$Zr_{70}Ni_{30}$	8.32	−1.30
$Zr_{75}Ru_{25}$	15.16	–
$Zr_{80}Rh_{20}$	–	−1.68
$Zr_{75}Rh_{25}$	12.98	−1.48
$Zr_{70}Rh_{30}$	–	−1.20
$Zr_{75}Pd_{25}$	9.19	–
$Zr_{80}Ir_{20}$	–	−1.47
$Zr_{75}Ir_{25}$	11.89	−1.35
$Zr_{70}Ir_{30}$	–	−1.34
$Zr_{80}Pt_{20}$	13.17	–
$Zr_{75}Pt_{25}$	9.88	–

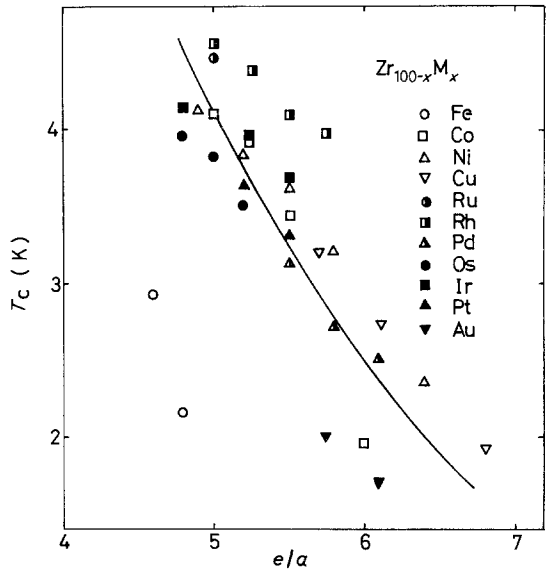

Figure 14 Relationship between T_c and the average outer electron per atom, e/a, for $Zr_{100-x}M_x$ (M = Fe, Co, Ni, Cu, Ru, Rh, Pd, Os, Ir, Pt or Au) amorphous alloys.

temperature coefficient in the temperature range above 12 K. The temperature dependence of resistance was found to be approximately represented by the following relations: (1) $-\ln T$ at temperatures between 16 and 30 K; (2) $-T^2$ at T = 30 to 70 K; and $-T$ at T = 150 to 250 K. In the range 12 to 250 K, $(R_{max} - R_{250})/R_{max}$ is about 3.6%. Table I summarizes the temperature, T_{max}, at which $R(T)$ of Zr–M (M = nickel, ruthenium, rhodium, palladium, iridium or platinum) amorphous alloys exhibits a maximum value. T_{max} tends to rise with increasing zirconium content for the series of $Zr_{100-x}Ni_x$ and $Zr_{100-x}Pt_x$ alloys and with the decrease in the group number of the M elements for a series of $Zr_{75}M_{25}$ (M = ruthenium, rodium or palladium) alloys. Additionally, Table I shows the temperature coefficient of resistivity (tcr), $1/R_{250}(dR/dT)$, in the temperature range of 150 to 250 K for Zr–M (M = cobalt, nickel, iridium or rhodium) amorphous alloys. The tcr values lie in the range -1.75×10^{-4} to -1.05×10^{-4} K^{-1} and its absolute values tend to increase with increasing zirconium content, in accordance with the tendency for the T_{max} and T_c values. Mooij [22] has reported that the crystalline and amorphous alloys with a residual resistivity above about 1.50 $\mu\Omega$ m exhibit a negative tcr. The residual resistivity of 4.2 K for the Zr–M amorphous alloys is in the range 1.80 to 1.90 $\mu\Omega$ m and their tcr values are negative, consistent with the Mooij's empirical rule.

4. Discussion

4.1. Correlation between T_c and the average outer electron per atom e/a

The compositional dependence of T_c for many superconductors has been known to be closely related to the change in the number of the average outer electron per atom (e/a). That is, there is a strong correlation between T_c and e/a and the correlation has been known as the Matthias rule [23] for crystalline superconductors and as the Collver–Hammond rule [24] for amorphous superconductors. The latter rule represents that T_c shows a maximum value at e/a = 6.4 for the 4d transition metals and alloys and at e/a = 6.8 for the 5d metals and alloys. The relation between T_c and e/a for all the Zr–M amorphous alloys examined in the present work is shown in Fig. 14. T_c tends to rise with decreasing e/a and one cannot recognize the tendency that T_c exhibits a maximum value at e/a = 6.4 or 6.8. Thus the change in T_c of the Zr–M amorphous alloys with the group number, period and content of M elements does not always agree with the Collver–Hammond curve [24] obtained only for metals and alloys of neighbouring metals. The rise of T_c of the Zr–M amorphous alloys with decreasing e/a implies that T_c is higher for the alloys containing M elements with a group number close to zirconium. It has been recently found for a number of melt-quenched amorphous superconductors consisting of transition metals [25–28] that the bare density of states for the d electrons at the Fermi level decreases with the increase in the difference in the group number between the constituent metals through the splitting of the d-band, resulting in a lower T_c. These recent data also show that the compositional dependence of T_c for the amorphous alloys often cannot be interpreted by the Collver–Hammond rule. Similarly, the reason why T_c of the Zr–M amorphous alloys is lower in the case where the group number of M elements is far away from zirconium is interpreted as due to the decrease in the electronic bare density of states at the Fermi level through the splitting of d-band.

4.2. Change in T_c with M content and its dominating factor

It was pointed out in Section 4.1 that a rather strong correlation between T_c and e/a, which may be attributed to the change in $N(E_f)$ with e/a, is recognized for the Zr–M amorphous alloys. However, T_c has been known [29] to correlate closely with the Debye temperature (θ_D) and the coupling constant between electron and phonon (λ), in additon to $N(E_f)$. In this subsection we shall evaluate the values of θ_D, $N(E_f)$

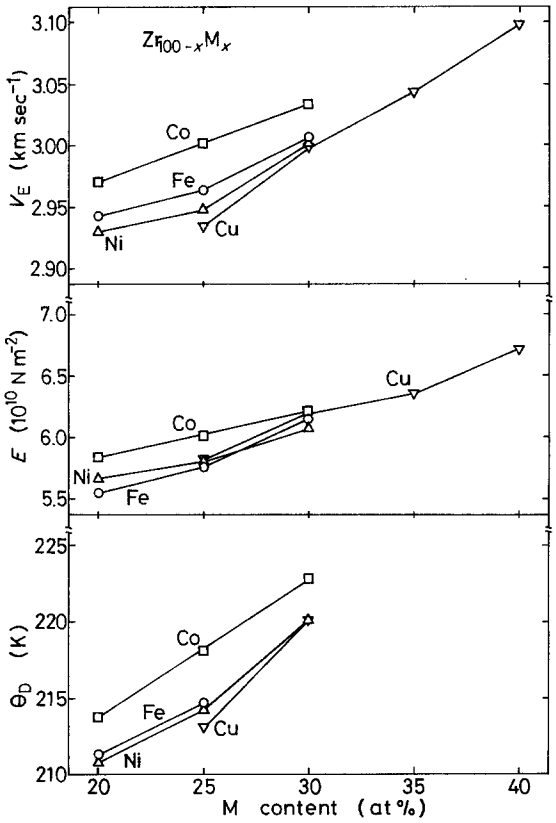

Figure 15 The Young's modulus sound velocity, V_E, Young's modulus, E, and Debye temperature, θ_D, of $Zr_{100-x}M_x$ (M = iron, cobalt, nickel or copper) amorphous alloys as a function of M content.

and λ for $Zr_{100-x}M_x$ (M = iron, cobalt, nickel or copper) amorphous alloys and investigate the correlation between T_c and these parameters.

The value of θ_D for an isotropic solid such as amorphous alloys is calculated from experimental values of Young's modulus, E, and density, d using the following relation [30, 31]:

$$\theta_D = \frac{h}{k_B}\left(\frac{9N}{4\pi}\right)^{1/3}\frac{E^{1/2}}{M^{1/3}d^{1/6}}f(\nu) \quad (1)$$

where N is Avogadro's number, M is the mean atomic weight and $f(\nu)$ is a function of Poisson's ratio, ν, and if ν is 0.40 commonly observed in amorphous alloys [32], $f(\nu) = 0.46$. Yhe θ_D values for the Zr–M amorphous alloys calculated from Equation 1 are plotted as a function of M content in Fig. 15. The θ_D value rises almost linearly in the range 210 to 220 K with increasing M content, contrary to the tendency of T_c, which decreases. Accordingly, the θ_D is not thought to be a dominating factor for T_c of the $Zr_{100-x}M_x$ amorphous alloys.

The electronic dressed density of states at the Fermi Level, $N(E_f)^* = N(E_f)(1 + \lambda)$, was estimated from the measured values of the H_{c2} gradient near T_c, $-(dH_{c2}/dT)_{T_c}$, and normal electrical resistivity, ϱ_n, by using the following formula which is derived from the Ginzburg– Landau–Abrikosov–Gorkov (GLAG) theory (e.g. [33]) and is applicable for the dirty-type superconductor of the Zr–M amorphous alloys:

$$N(E_f)(1 + \lambda) = -\frac{\pi}{8k_B e\varrho_n}\left(\frac{dH_{c2}}{dT}\right)_{T_c} \quad (2)$$

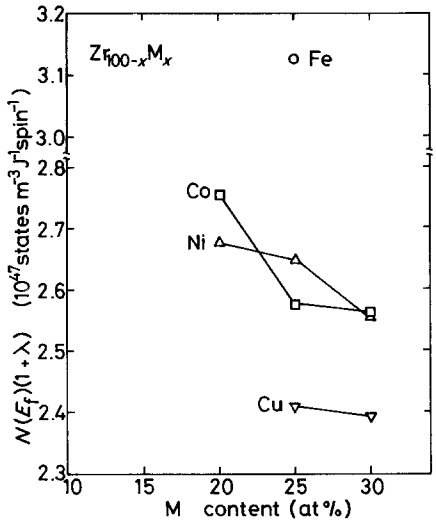

Figure 16 The dressed density of states at the Fermi level, $N(E_f)$ $(1 + \lambda)$, of $Zr_{100-x}M_x$ (M = iron, cobalt, nickel or copper) amorphous alloys as a function of M content.

The values of $N(E_f)(1 + \lambda)$ for the Zr–M amorphous alloys thus obtained are plotted as a function of M content in Fig. 16. The $N(E_f)(1 + \lambda)$ value tends to decrease as does T_c (see Fig. 3) with increasing M content, suggesting that T_c is dominated by $N(E_f)$ and/or λ rather than θ_D.

Subsequently, each parameter of λ and $N(E_f)$ was evaluated separately in order to investigate which parameter, $N(E_f)$ or λ, dominates the M concentration dependence of T_c. λ can be estimated from the T_c and θ_D values by using the McMillan equation [29],

$$\lambda = \frac{1.04 + \mu^* \ln(\theta_D/2.45T_c)}{(1 - 0.62\mu^*)\ln(\theta_D/1.45T_c) - 1.04} \quad (3)$$

where μ^* is the Coulomb pseudopotential and the value of μ^* for Zr–M amorphous alloys consisting of sition metals has been reported to lie in the range 0.10 to 0.15 for the transition metals and alloys [34] and is reasonably assumed to be $\simeq 0.13$. While, $N(E_f)$ is calculated from the measured values of ϱ_n and $-(dH_{c2}/dT)_{T_c}$ and the estimated value of λ by using Equation 2. The λ and $N(E_f)$ values derived thus are plotted as a function of M content in Figs. 17 and 18, respectively. From the comparison of Figs. 3, 17 and 18, one can notice a better similarity of the compositional dependence between T_c and λ as compared with that of T_c and $N(E_f)$, indicating that λ may be

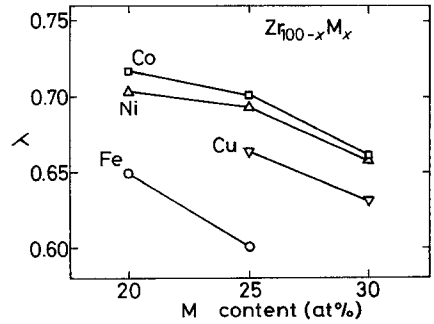

Figure 17 The electron–phonon coupling constant, λ, of $Zr_{100-x}M_x$ (M = iron, cobalt, nickel or copper) amorphous alloys as a function of M content.

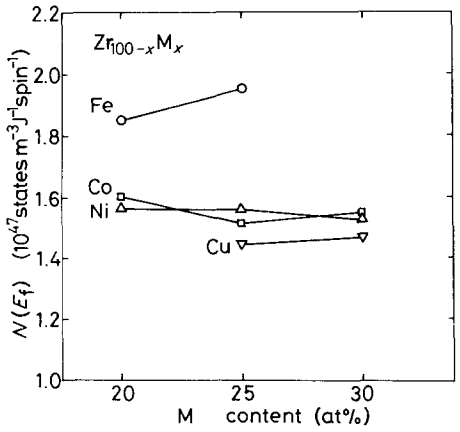

Figure 18 The bare density of states at the Fermi level, $N(E_f)$, of $Zr_{100-x}M_x$ (M = iron, cobalt, nickel or copper) amorphous alloys as a function of M content.

concluded to be the most dominant factor for the change in T_c with M content for the Zr–M amorphous superconductors.

The relation between λ and the phonon frequency ω is expressed by the Eliashberg equation, which gives the accurate numerical solution of T_c, as follows [29]:

$$\lambda = 2\int_0^\infty \alpha^2(\omega)F(\omega)\,d\omega/\omega \quad (4)$$

Here $F(\omega)$ is the phonon spectrum and $\alpha(\omega)$ the electron–phonon matrix element. Although there is no information available on the change in the quantity $\alpha^2(\omega)F(\omega)$ for the Zr–M amorphous alloys with M content, the change in λ with M content can be inferred by using McMillan's factorization of λ [29],

$$\lambda = \frac{N(E_f)\langle I^2\rangle}{A\langle\omega^2\rangle} \quad (5)$$

Here $\langle I^2\rangle$ is the average over the Fermi surface of the square of the electronic matrix element, A the average ionic mass and $\langle\omega^2\rangle$ an average of the square of the phonon frequency. As shown in Fig. 15, the Young's modulus sound velocity V_E, Young's modulus E and θ_D for the Zr–M amorphous alloys increase with increasing M content, but no significant change in $N(E_f)$ with M content (Fig. 18) is recognized. The Debye approximation [35] represents the following relation between V_E and ω_D or θ_D:

$$V_E = \omega_D\left(\frac{6\pi^2N}{\Omega}\right)^{-1/3} = \frac{k_B\theta_D}{\hbar}\left(\frac{6\pi^2N}{\Omega}\right)^{-1/3} \quad (6)$$

where N/Ω is the number of atoms per unit volume and $\hbar$ is Planck's constant. Equation 6 indicates that the increase in V_E with M content is also related to the increase in ω_D as well as θ_D. From the above-described discussion, the decrease in λ with increasing M content for the Zr–M amorphous alloys is said to originate from the increase in $\langle\omega^2\rangle$ with M content, even though there is no established information on the compositional dependence of $\langle I^2\rangle$.

4.3. Change in T_c with the group number and period of M elements and its dominating parameter

In Section 4.2 we investigated the dominating parameters for the change in T_c with M content for the

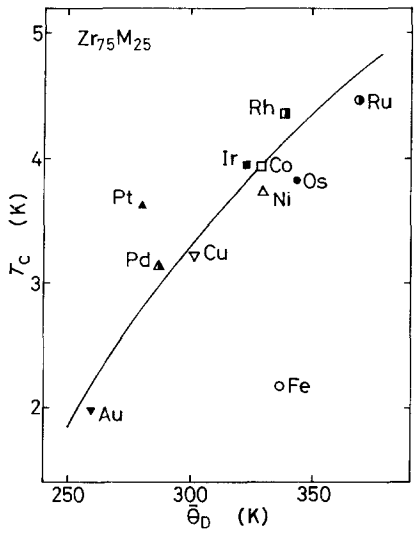

Figure 19 Relationship between T_c and weighted average Debye temperature, $\bar{\theta}_D$, for $Zr_{75}M_{25}$ (M = Fe, Co, Ni, Cu, Ru, Rh, Pd, Os, Ir, Pt or Au) amorphous alloys.

$Zr_{100-x}M_x$ amorphous alloys. In this section we shall examine the correlation between T_c and θ_D, $N(E_f)$ or λ for the series of $Zr_{75}M_{25}$ amorphous alloys with an aim to clarify the reason for the change in T_c with the group number and periodicity of M elements. Fig. 19 shows the relation between T_c of the $Zr_{75}M_{25}$ amorphous alloys and the weighted mean Debye temperature

$$\bar{\theta}_D = \sum \frac{X_i}{100}\theta_{D,i} \quad (7)$$

for the pseudo binary Zr–M alloys. Here $\theta_{D,i}$(M) values are the Debye temperature of the transition M metals and X_i is the atomic concentration of Zr and M metals. As can be seen in Fig. 19, T_c and $\bar{\theta}_D$ show a strong correlation; T_c rises significantly with rising $\bar{\theta}_D$. Also in Fig. 20, the relation between T_c and $N(E_f)(1+\lambda)$ for the $Zr_{75}M_{25}$ amorphous alloys is shown. Although a relatively large scattering is seen, one can see a clear tendency that T_c rises with increasing $N(E_f)(1+\lambda)$. It appears important to point out that the relation between T_c and θ_D for the $Zr_{75}M_{25}$ amorphous alloys with M elements belonging to different group number and period is distinct from the

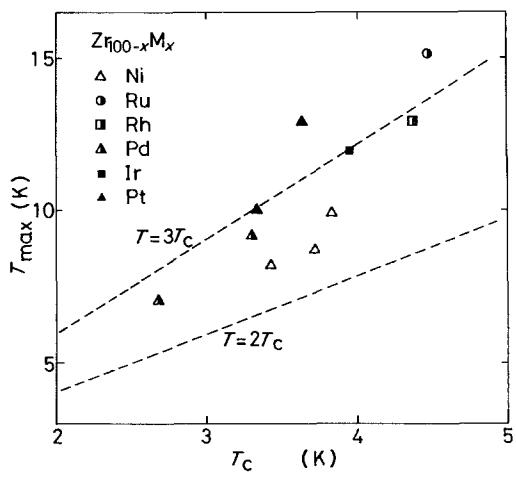

Figure 20 Relationship between T_c and the dressed density of states at the Fermi level, $N(E_f)(1+\lambda)$, for $Zr_{100-x}M_x$ (M = Fe, Co, Ni, Cu, Ru, Rh, Os, Ir, Pt or Au) amorphous alloys.

case discussed in Section 4.2. In the relationship between T_c and $\bar{\theta}_D$ for the $Zr_{75}M_{25}$ amorphous alloys, T_c rises with rising $\bar{\theta}_D$, i.e. with the increase in $\langle\omega^2\rangle$. This suggests that the changes in the group number and period of the M elements cause a significant variation of $N(E_f)$ which reflects in the similar variation of λ, resulting in the strong correlation between T_c and $N(E_f)$ $(1 + \lambda)$ represented in Fig. 20. The conclusion derived in this section, i.e. the variation of T_c for the $Zr_{75}M_{25}$ amorphous alloys with M elements originates from $N(E_f)$, is consistent with the inferrence derived from the relation between T_c and e/a represented in Section 4.1.

4.4. Temperature dependence of electrical resistivity

It has been known (e.g. [36]) that the temperature dependence of electrical resistivity for amorphous alloys is roughly divided into the following three categories. One is the ln T dependence of resistivity in the temperature range lower than about 20 K. The second is the existence of the temperature region where the resistance varies with T^2 and/or $1 - T^2$, and the third is the linear dependence of resistivity as a function of temperature. The $R(T)$ of all the Zr–M amorphous alloys measured in the present work was found to change in the order of $-\ln T$, $1 - T^2$ and $-T$ with rising temperature, being consistent with the previous results for amorphous Zr–M (M = cobalt [37], nickel [37] or copper [11]) alloys, even though the transition temperature at which the temperature dependence of R changes, does not always agree with each other.

4.5. Correlation between T_c and T_{max}

It was found for all the superconducting amorphous alloys measured in the present work that electrical resistance exhibits a maximum value at low temperatures ranging from about 6 to 15 K. The reason for the hump phenomenon in the R–T relationship for amorphous superconductors has been considered as follows [38, 39]; the local fluctuation leading to an appearance of superconductivity begins to generate at T_{max} and the number of the superconducting fluctuations increases with lowering temperature, resulting in a drastic decrease in $R(T)$. That is, T_{max} is defined as the temperature at which the superconducting fluctuation begins to appear locally and hence one may expect a strong correlation between T_{max} and T_c. As expected, Fig. 21 indicates a clear tendency that T_{max} lies in the range between $2T_c$ and $3T_c$. A similar hump phenomenon in which the electrical resistance exhibits a maximum value has been also found [40] for the non-superconducting Zr–M amorphous alloys such as $Zr_{70}Mn_{30}$ etc. However, the T_{max} for such amorphous alloys shows much higher values ($\simeq 30$ K) as compared with those for superconducting amorphous alloys, probably because of a different mechanism for the appearance of T_{max}.

4.6. Correlation between tcr and superconducting characteristics

Fig. 22 shows the relationship between T_c and tcr for Zr–M (M = cobalt, rhodium or iridium) amorphous alloys. One can see a clear tendency between both these parameters; the larger the negative values of tcr the higher is the T_c. This differs from the previous results [41] for zirconium–metalloid amorphous alloys such as Zr–Si and Zr–Ge etc. in which T_c decreases with the increasing ϱ_n and the negative value of tcr. It suggests that the effect of solute element on the superconducting properties is not always the same between transition metal and metalloid. It has been reported for noble metal-based crystalline alloys [42] that tcr is closely related to λ which is a dominating factor for T_c. Fig. 23 shows the relationship between tcr and λ for Zr–M (M = cobalt or nickel) amorphous alloys. It can be seen that λ increases almost linearly with increasing tcr. From the strong correlation between λ and tcr, the reason why T_c of the Zr–M amorphous alloys rises with the negative value of tcr is reasonably thought to originate from the increase in λ.

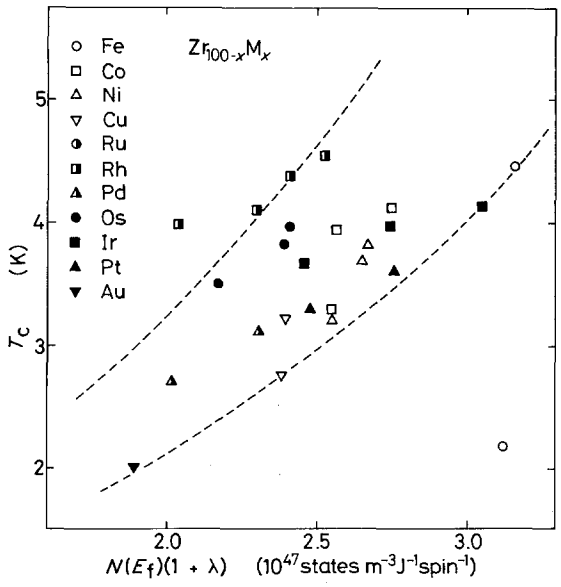

Figure 21 Relationship between T_c and T_{max} for $Zr_{100-x}M_x$ (M = nickel, ruthenium, palladium, iridium or platinum) amorphous alloys.

5. Conclusion

Superconducting and electrical properties of zirconium–transition metal (M = Fe, Co, Ni, Cu, Ru, Rh, Pd, Os, Ir, Pt or Au) binary amorphous alloys

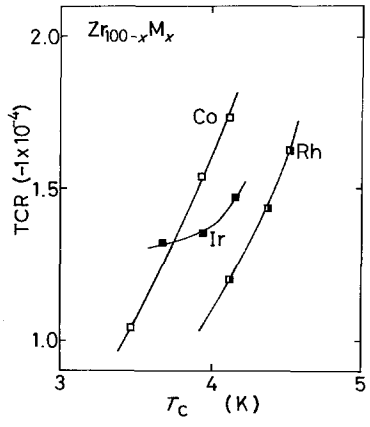

Figure 22 Relationship between T_c and tcr for $Zr_{100-x}M_x$ (M = cobalt, rhodium or iridium) amorphous alloys.

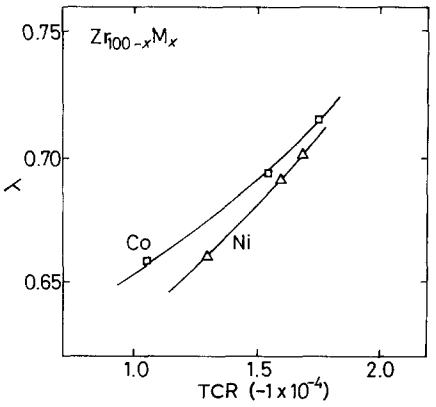

Figure 23 Relationship between tcr and λ for $Zr_{100-x}M_x$ (M = cobalt or nickel) amorphous alloys.

were examined with an aim to clarifying the effect of M elements on both the properties. The results obtained are summarized as follows:

1. The formation range of the amorphous phase extends in the vicinity of a eutectic composition ($\simeq$ 75 at % Zr) and becomes narrower in the order Ni > Fe $\simeq$ Co > Cu > Rh > Pd $\simeq$ Os $\simeq$ Ir $\simeq$ Au > Pt > Ru.

2. The Zr–M amorphous alloys exhibit a very sharp transition from normal to superconducting state and the transition temperature, T_c, rises with decreasing M content for $Zr_{100-x}M_x$ alloys and in the order of Ru > Rh > Ir > Co > Os > Ni > Pt > Cu > Pd > Fe > Au for $Zr_{75}M_{25}$ alloys. That is, T_c tends to exhibit higher values when the M elements belong to the same period as zirconium and have a smaller group number. The alloys exhibiting T_c higher than the boiling temperature of liquid helium ($\simeq$ 4.2 K) are limited to $Zr_{80}Rh_{20}$ (T_c = 4.55 K), $Zr_{75}Rh_{25}$ (4.38 K) and $Zr_{75}Ru_{25}$ (4.47 K). Whilst the change in T_c with M content originates from the variation of λ through ω, the change in T_c with the period and group number of M elements is interpreted to be dominated by the variation of λ through $N(E_f)$.

3. J_c is as low as $\simeq 10^6 A\,m^{-2}$ at T = 1.40 K and H = 0 even for $Zr_{80}Rh_{20}$ exhibiting the highest T_c value, leading to the conclusion that the fluxoid pinning force in the Zr–M amorphous alloys is extremely weak because of a homogeneous structure on the scale of coherence length. $H_{c2}(T)$ shows a linear temperature dependence at temperatures near T_c and the gradient, $-(dH_{c2}/dT)_{T_c}$, possesses a large value above 2.5 T K^{-1}. The gradient tends to increase with increasing zirconium content.

4. A large resistive state due to the flux flow phenomenon appears in the transition from superconducting to normal states in sweeping field, but the flux flow resistance disappears completely at high fields just below H_{c2}. The recovery phenomenon into a superconducting state was found to occur more distinctly for the Zr–M alloys containing M element such as iron or cobalt and its reason was interpreted to originate from the suppression of the pair-breaking action due to the magnetic scattering arising from the magnetic element by the application of high field.

5. The hump phenomenon of electrical resistance in the resistance–temperature relationship, probably because of a generation of the superconducting fluctuations, was found to occur in the temperature range of $2T_c$ to $3T_c$ and the temperature at which the resistance exhibits a maximum value tends to rise with rising T_c.

6. The temperature dependence of the electrical resistance is expressed by each relation of $-\ln T$ at temperatures below 30 K, $-T^2$ in the range 30 to 80 K and $-T$ in the range of 150 to 250 K. The tcr, $1/R_{250}(dR/dT)$, in the range 150 to 250 K shows negative values ranging from 1.05×10^{-4} to $1.75 \times 10^{-4}\,K^{-1}$. It was found a clear tendency that the larger negative value of tcr the larger is the λ and the higher is the T_c.

References

1. O. RAPP, B. LINDBERG, H. S. CHEN and K. V. RAO, *J. Less-Common Metals* **62** (1978) 221.
2. M. TENHOVER and W. L. JOHNSON, *Physica* **108B** (1981) 1221.
3. M. G. KARKUT and R. R. HAKE, *Bull. Amer. Phys. Soc.* **27** (1982) 156.
4. O. RAPP, M. FLODIN, A OSTLAND and H. FREDRIKSSON, *Phys. Scripta* **25** (1982) 804.
5. M. TENHOVER and W. L. JOHNSON, *Phys. Rev.* **B27** (1983) 1610.
6. V. L. MOROZZI, P. OELHAFEN, A. R. WILLIAMS, H. J. GUNTHERODT and J. KUBLER, *ibid.* **B27** (1983) 2049.
7. S. J. POON and W. L. CARTER, *Solid State Commun.* **35** (1980) 249.
8. A. RAVEX, J. C. LASJAUNIAS and O. BETHOAX, *ibid.* **40** (1981) 853.
9. E. BABIC, R. RISTIC, M. MILJAK, M. G. SCOTT and G. GREGAN, *ibid.* **39** (1981) 139.
10. A. C. ANDERSON, C. C. KOCH and J. O. SCARBROUGH, *Phys. Rev.* **B26** (1982) 1156.
11. K. SAWER and H. LOHNEYSEN, *ibid.* **B26** (1982) 107.
12. K. TOGANO and K. TACHIKAWA, *J. Appl. Phys.* **46** (1975) 3609.
13. A. J. DREHMAN and W. L. JOHNSON, *Phys. Status Solidi (a)* **52** (1979) 499.
14. A. INOUE, Y. TAKAHASHI, A. HOSHI, U. MIZUTANI and T. MASUMOTO, *J. Phys. E Sci. Instrum.* **17** (1984) 546.
15. Aishin-Seiki Co Ltd, Kariya 448, Japan, Commercial Catalogue (1985).
16. L. R. TESTARDI, J. T. KRAUSE and H. S. CHEN, *Phys. Rev.* **B8** (1973) 4464.
17. C. J. SMITHELLS and E A BRANDES, in "Metals Reference Book", 5th Edn (Butterworths, London, 1976).
18. H. A. DAVIES, in "Amorphous Metallic Alloys", edited by F. E. Luborsky (Butterworths, London, 1983) p. 80.
19. Y. B. KIM, C. F. HEMPSTEAD and A. R. STRNAD, *Phys. Rev.* **139** (1965) A-1163.
20. N. TOYOTA, T. FUKASE, A. INOUE, Y. TAKAHASHI and T. MASUMOTO, *Physica* **107B** (1981) 465.
21. N. TOYOTA, A. INOUE, T. FUKASE and T. MASUMOTO, *J. Low Temp. Phys.* **55** (1984) 393.
22. J. H. MOOIJ, *Phys. Status Solidi* **A17** (1973) 521.
23. B. T. MATTHIAS, in "Progress in Low Temperature Physics", Vol. 2 (Interscience, New York, 1957) p. 139.
24. M. M. COLLVER and R. H. HAMMOND, *Phys. Rev. Lett.* **30** (1973) 92.
25. *Idem, Solid State Commun.* **22** (1977) 55.
26. T. MASUMOTO, A. INOUE, S. SAKAI, H. M. KIMURA and A. HOSHI, *Trans. Jpn. Inst. Metals* **21** (1980) 115.
27. A. INOUE, Y. TAKAHASHI, N. TOYOTA, T. FUKASE and T. MASUMOTO, *J. Mater. Sci.* **18** (1983) 114.
28. *Idem, Trans. Jpn. Inst. Metals* **23** (1982) 693.

29. W. L. McMILLAN, *Phys. Rev.* **167** (1968) 331.
30. F. H. HERBSTEIN, *Adv. Phys.* **10** (1961) 318.
31. C. C. KOCH, D. M. KROEGER, J. O. SCARBROUGH and B. C. GIESSEN, *Phys. Rev.* **B22** (1980) 5213.
32. H. S. CHEN and K. A. JACKSON, in "Metallic Glasses", edited by H. J. Leamy and J. T. Gilman, (ASM, Metals Park, Ohio, 1978) p. 84.
33. T. P. ORLANDO, E. J. MCNIFF Jr, S. FORNER and M. R. BEASLEY, *Phys. Rev.* **B19** (1979) 4545.
34. K. H. BENNEMANN and J. W. GARLAND, in "Superconductivity in d- and f-band Metals", edited by D. H. Douglass, AIP Conference Proceedings no. 4 (AIP, New York, 1972) p. 116.
35. T. OTSUKA, "Ferroelectrics and Superconductor" (The Japan Institute of Metals, Sendai, 1973) p. 131.
36. U. MIZUTANI, *Solid Phys.* **15** (1980) 460.
37. K. H. BUSHOW and N. M. BEEKMANS, *Phys. Rev.* **19** (1979) 3846.
38. W. L. JOHNSON, C. C. TSUEI and P. CHAUDHARI, *ibid.* **B17** (1978) 2884.
39. N. TOYOTA, A. INOUE, K. MATSUZAKI, T. FUKASE and T. MASUMOTO, *J. Phys. Soc. Jpn.* **53** (1984) 924.
40. M. TENHOVER and W. L. JOHNSON, *Physica* **B180** (1981) 1221.
41. A. INOUE, T. MASUMOTO and H. S. CHEN, *J. Phys. F Met. Phys.* **13** (1983) 2603.
42. O. RAPP and M. FLODIN, *Phys. Rev.* **B26** (1982) 99.

Received 29 April
and accepted 10 June 1985